31st Annual International Conference of the IEEE EMBS
Minneapolis, Minnesota, USA, September 2-6, 2009

Experimental Setup for Developing Acousto-Electric Interaction Imaging

Mathieu Gendron, Robert Guardo and Michel Bertrand

***Abstract*— Acousto-Electric Interaction (AEI) is a physical phenomenon identified in the literature as potentially useful for imaging the electrical conductivity of biological tissues. AEI could lead to a non-invasive technique for detecting breast tumors, since the conductivity of pathological tissues differs significantly from the conductivity of healthy breast tissues. Applying AEI to image heterogeneous structures of the size of the breast represents a major technical challenge. We present in this paper an experimental setup designed to address the various instrumentation issues of AEI. Tests results are presented showing the ultrasonic vibration potential (also known as the Debye effect) and the AEI signals. A preliminary analysis of the AEI signal we recorded suggests that cavitation effects can be measured with this technique.**

I. INTRODUCTION

Acousto-Electric Interaction has been suggested as a technique for imaging the electrical conductivity distribution of biological tissues with a resolution typical of ultrasound [1], [2], [3], [4]. It has been shown that breast tumors have characteristic electrical properties different from those of healthy tissue [5]. Based on this difference, imaging the electrical conductivity of the breast could help identify tumors. To perform non-invasive imaging of the breast, AEI must be able to accurately measure conductivity in an organ several centimeters in diameter. Until now, most studies on AEI have been made with electrolytic solutions contained in small measurement cells of the order of a millimeter or so [1], [3], [6]. Even in those conditions AEI signals are very small, perhaps in the order of hundreds of microvolts; and since their amplitude decreases as the size of the cell increases [6], signals in the range of microvolts could be expected for the larger "measurement cell" associated with a breast cancer detection based on AEI imaging. Therefore for such an application, a very high sensitivity measurement system would be required. For the design of such a system, critical issues related to signal conditioning, interference control, common mode rejection, stability with respect to electrode conditions, etc. need to be addressed. Interestingly, several aspects of this problem are similar to those encountered in electrical impedance tomography (EIT).

In this paper, we present an experimental setup with the instrumentation used and the methods applied to acquire small AEI signals under well-controlled experimental conditions. The purpose here is to establish the fundamentals that will serve in the design of an AEI electrical conductivity imaging system for breast cancer detection. The model used for relating the AEI signal to conductivity and to the experimental variables is presented in section II. Section III describes the experimental setup and the acquisition sequence. Test results are presented in section IV.

M. Gendron is with the Institute of Biomedical Engineering, Department of Electrical Engineering, Ecole Polytechnique de Montreal, Montreal, Quebec, Canada gendron@igb.polymtl.ca

R. Guardo is with the Institute of Biomedical Engineering, Department of Electrical Engineering, Ecole Polytechnique de Montreal, Montreal, Quebec, Canada guardo@igb.polymtl.ca

M. Bertrand is with the Institute of Biomedical Engineering, Department of Electrical Engineering, Ecole Polytechnique de Montreal, Montreal, Quebec, Canada bertrand@igb.polymtl.ca

II. THEORY

The voltage $V = V(x,y,z)$ measured by a pair of electrodes, called a lead, has been shown to be [3]:

$$V = \iiint \rho(\tilde{\mathbf{J}}^L \cdot \mathbf{J}^I)dxdydz \tag{1}$$

where $\rho = \rho(x,y,z)$ is the electrical resistivity, $\tilde{\mathbf{J}}^L = \tilde{\mathbf{J}}^L(x,y,z)$ is the lead field of the measurement electrodes using a unit current and $\mathbf{J}^I = \mathbf{J}^I(x,y,z)$ is the lead field of the current injecting electrodes. Since $\mathbf{J} = -\sigma\nabla\varphi$, (1) can be equivalently written as:

$$\begin{aligned} V &= \iiint \frac{1}{\sigma}(-\sigma\nabla\varphi^L \cdot -\sigma\nabla\varphi^I)dxdydz \\ &= \iiint \sigma(\nabla\varphi^L \cdot \nabla\varphi^I)dxdydz \end{aligned} \tag{2}$$

where $\sigma = \sigma(x,y,z) = 1/\rho$ is the electrical conductivity and $\varphi = \varphi(x,y,z)$ is the electrical potential.

The modulation of the electric conductivity σ_0 by an acoustic pressure ΔP has been described in [7], [8]:

$$\frac{\Delta\sigma}{\sigma_0} = K_I \Delta P \tag{3}$$

where $\Delta\sigma$ is the variation in conductivity and K_I a proportional constant dependent on the solvent of the electrolytic solution and the ions. In a 0.9% NaCl solution, K_I is of the order of $10^{-9}\mathrm{Pa}^{-1}$.

With an acoustic pressure ΔP, the resulting electrical conductivity σ will be:

$$\sigma = \sigma_0 + K_I\sigma_0\Delta P \tag{4}$$

Substituting (4) in (2) gives:

$$\begin{aligned} V &= \iiint (\sigma_0 + K_I\sigma_0\Delta P)(\nabla\varphi^L \cdot \nabla\varphi^I)dxdydz \\ &= \underbrace{\iiint \sigma_0(\nabla\varphi^L \cdot \nabla\varphi^I)dxdydz}_{V^{LF}} \\ &\quad + \underbrace{\iiint (K_I\sigma_0\Delta P)(\nabla\varphi^L \cdot \nabla\varphi^I)dxdydz}_{V^{AE}} \end{aligned} \tag{5}$$

978-1-4244-3296-7/09/$25.00 ©2009 IEEE

The first term, V^{LF}, represents the signal component independent of the acoustic perturbation. The second term, V^{AE}, is dependent of the acoustic perturbation and can be isolated by filtering the measurement V in order to determine σ_0.

With an ultrasonic oscillatory pressure perturbation located within the domain of sensitivity of the leads, we can see that the amplitude of the signal caused by the acoustic perturbation will tend to vanish because of the integral over the domain [6].

III. MATERIALS AND METHODS

A. General description

The experimental setup is shown in Fig. 1. A water tank filled with degassed water contains an ultrasound transducer and an AEI measurement cell. A pressure wave originating from the transducer sets the AEI in the measurement cell. This cell consists of a sealed cavity filled with a 0.9% NaCl electrolytic solution, and of a watertight chamber. This chamber contains parts of the front-end electronics required to apply the excitation current and to sense the resulting voltage at the measurement electrodes. An electronic unit outside the water tank contains the remaining current injection and voltage measurement circuits. We chose this layout so that the current drivers and the voltage pre-amplifiers can be located close to the electrodes. This enables preserving a high output impedance for the current drivers and a high input impedance for the pre-amplifiers.

B. Measurement cell

The measurement cell, shown in Fig. 2, comprises the following components:

1) Watertight chamber: This chamber is designed to hold a 35.6 $\times$ 25.4 mm^2 printed circuit board (PCB) containing the pre-amplifiers and the current drivers.

2) Electrolytic cavity: The bottom part of the measurement cell contains the electrolytic solution which is insonated. The size of the electrolytic cavity is determined by the "U" shaped frame placed on the bottom part and held by screws. In the present setup, the frame produces a cavity of 42.0 $\times$ 10.0 $\times$ 6.9 mm^3. This cavity is closed by two acoustic windows made of 0.05 mm thick adhesive tape. These windows are virtually transparent to the acoustic signals and serve two purposes. One is to be able to use a range of electrolytic fluid solutions without having to change the fluid in the whole water tank. The other has to do with the lead field: being an insulator in the frequency range we are studying, the adhesive tape confines the lead field of the electrodes to the electrolytic cavity.

3) Cavity fluid inlet and outlet: Two threaded holes located on the top part of the electrolytic cavity receive plastic tubes used to fill/drain the cavity with the electrolytic solution. This tubing provides an easy way to replace the solution by another during the acquisition session. This can serve to verify how the AEI signal is affected by modifying the electrical conductivity of the solution either by changing the ionic concentration or by changing the nature of the ions.

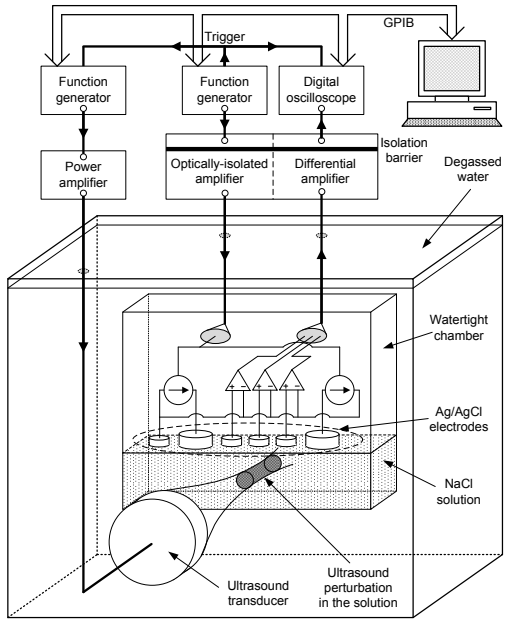

Fig. 1. Experimental setup

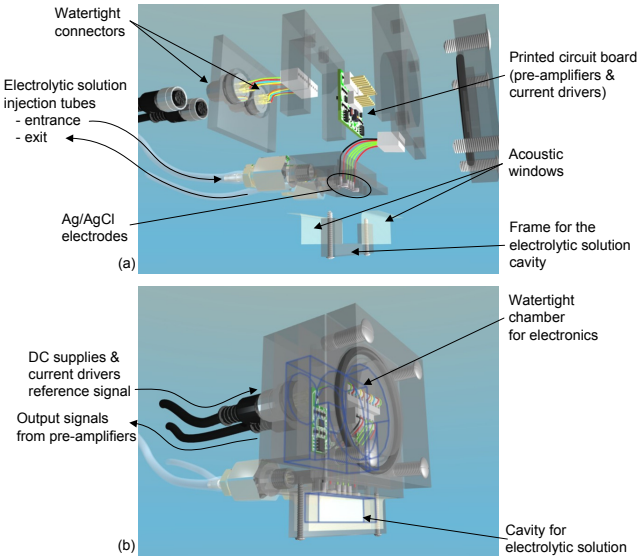

Fig. 2. The AEI measurement cell. (a) disassembled view. (b) assembled view.

Also, instead of only using an electrolytic solution, one can place a phantom (a gel, for example) in part of the cavity.

4) Electrodes: Six Ag/AgCl electrodes are located on the top part of the electrolytic cavity. One electrode (2.1 mm diameter) is the ground/reference, two electrodes (4.2 mm diameter) are dedicated to current injection, and the remaining three electrodes (2.1 mm diameter) are for measuring potential differences. As shown in the diagram of the experimental setup (Fig. 1), the three voltage measurement electrodes are connected to pre-amplifiers located within the watertight chamber. The output signals from these pre-amplifiers are transmitted by a 1.5 m long cable to a differential amplifier (DA) module located with the rest of the system electronics.

The pair of signals entering the differential amplifier is selected through switches on the module's front panel. These switches provide a choice of 3 differential signals, originating from pairs of electrodes with different spacing. This system feature will be used to investigate the effect of electrode separation on the characteristics of the AEI signal.

Ag/AgCl electrodes were chosen to avoid polarization since we need to apply a relatively high current density at low frequency.

C. Ultrasound transducer

We used a single-element ultrasound transducer (H-101 S/N -080, Sonic Concepts Inc., Bothell, WA) with an active diameter of 64.00 mm and a curvature radius of 62.64 mm. The central frequency was 1.078 MHz in the fundamental mode. The transducer is used with an impedance matching network. The focus has a full width at half maximum (FWHM) of 1.75 mm and a focal length of 13 mm, which we measured with a 1.0 mm diameter needle hydrophone (Precision Acoustics Ltd., Dorchester, Dorset, United Kingdom). We used a sound pressure of about 5 MPa at the focus.

The signal driving the transducer comes from a RF power amplifier (BBS0D3FOQ, Empower RF Systems Inc., Inglewood, CA), itself driven by a function generator (33220A, Agilent Technologies Inc., Santa Clara, CA). A burst of 8 sinusoidal periods at 1.078 MHz is used.

D. Current drivers

The current drivers comprise two circuits: a) an optically-isolated amplifier (OIA) and b) two differential inputs voltage-controlled current sources (VCCS). The OIA is built on the same PCB as the differential amplifier described in section III-E below, while the VCCS and the measurement electrodes pre-amplifiers share the small PCB located in the watertight chamber. The input signal for the OIA is provided by a programmable function generator (33220A, Agilent). The output of the OIA drives the two VCCS in phase opposition, creating a current source and a current sink at the outermost electrodes. With this drive arrangement, current flows primarily between those two electrodes, providing a predictable excitation lead field. However, as excitation frequency is increased, circuit asymmetries in the VCCS cause an imbalance current flow through the ground electrode. This distorts the excitation lead field and creates a common mode potential that may add some error to the voltage difference measurements. Proper selection of the frequency and amplitude of the excitation current is therefore critical to achieving optimal system performance. The experiments reported in this paper were done with a sinusoidal current of 6 $\mathrm{mA_{peak}}$ at 100 Hz. These values were chosen because, with our circuits, they provide a highly symmetrical current waveform that prevents electrode polarization and electrolysis of the solvent. Also, the relatively low frequency gives observation windows of 70 μs at each peak of the sine wave, within which the current amplitude varies less than 0.1%. These windows are sufficiently long to allow emitting bursts of 8 ultrasound pressure waves at 1.078 MHz and recording the resulting AEI signal.

E. Differential amplifier

The differential amplifier also consists of two parts. The pre-amplifiers are located close to the electrodes in the watertight chamber. The differential amplifier is in a plastic case close to the oscilloscope (TDS 3052B, Tektronix Inc., Beaverton, OR) which is used both for display and for digitizing the signals. The differential amplifier is isolated from the other circuits by a wideband transformer.

The differential amplifier has a voltage gain of 34 dB and a -3 dB bandwidth of 40 kHz to 2.5 MHz.

F. Data acquisition

Precise measurement of AEI signal requires the removal of the signal contributed by the Debye effect [1]. Since the Debye effect is independent of the applied current while the AEI signal amplitude is linearly dependent on the current [1], we can remove the Debye effect contribution by subtracting two signals acquired with different current polarities. We acquire a first signal at the positive peak of the current waveform and subtract from it the signal acquired at the negative peak of the current waveform.

A quiescent signal which is dependent of the current phase has been observed in our experimental setup. Presently, we do not know its origin; we hypothesize it is the same signal other authors have labeled "common-mode interference" [3]. Similar to what is done in [3], we subtract the quiescent signal (i.e. the one acquired while the transducer is not driven) from the AEI signal (i.e. while the transducer is driven). As will be shown below, our acquisition protocol enables us to track this quiescent signal for each current polarity.

The signal acquisition sequence is summarized in Table I.

TABLE I
ACQUISITION SEQUENCE.

Acquisition #	Current applied	Ultrasound applied
1	+I	yes
2	+I	no
3	-I	yes
4	-I	no
5	0	yes

Acquisitions 1 and 3 are those of AEI signals, acquired respectively at positive and negative peaks of the current waveform. Acquisitions 2 and 4 are those of the quiescent signals (without ultrasound applied) also at each current polarity. Acquisition 5 is for the measurement of the Debye effect (no current applied, but with ultrasound applied).

For each of the five acquisitions, we average 128 events with the oscilloscope before transferring the data to the computer. This process is repeated 4 times.

The function generators and the oscilloscope are controlled by GPIB ports with a graphical interface developed in LabVIEW (National Instruments Corporation, Austin, TX).

IV. RESULTS AND DISCUSSION

A. Experimental results

Fig. 3 shows the results of a sequence of acquisitions taken as described above. It shows the averaged raw signals and the resulting AEI signal. The average values are that of the five sets of 512 signals (from the four sequences of 128 events). The acquisitions listed in Table I are numbered 1 to 5 in the figure. Plots numbered 6 to 8 are those of processed results.

Plots #1 and #3 show the signals acquired while both current and ultrasound are applied. Their amplitude before amplification is in the order of hundreds of microvolts. This is similar to the results presented in [1]. Notice the expected change in signal polarity with current polarity. However we also note other differences in the waveforms which do not appear to be negative replica of each other. This can be explained by the presence of the Debye effect, which is independent of the applied current.

Plots #2 and #4 show the quiescent signals acquired for each current polarity. The amplitude of the quiescent signals is small compared to the amplitude of the raw AEI signals, although we have observed that is not always the case. Nevertheless, here, their effects are not insignificant, as can be observed in plots #6 and #7. Those plots are respectively quiescent signal 2 subtracted from signal 1, and signal 4 subtracted from signal 3. Indeed at time 65 μs, one could see that a 80 microvolts "transient" is present which is not related to acoustic stimulation. We can make similar observations at time 40 μs, although in this case it is less obvious. The origin of this quiescent signal is yet unexplained.

Plot #5 shows the Debye effect signal, i.e. the one acquired when no current is applied while however the acoustic sinusoidal burst propagates. The duration of the Debye signal appears much longer than the 8 cycles used for acoustic perturbation. This is due in part to the size of the sensitivity region of the measurement electrodes being much longer than an ultrasound wavelength.

Plot #8 is the AEI signal we derived from the above measurements. We can clearly see a dominant component corresponding to the 8 ultrasonic cycles. Some obvious non linear effects are present, in that the sinusoidal electrical drive to the transducer does not translate into a sinusoidal burst of AEI signal. This likely originates from non linear acoustic conditions, the pressure amplitude being in the range of 5 MPa. A ninth cycle follows the 8 cycles drive; this is due to the limited bandwidth of the transducer. We hypothesize this signal is due to cavitation effects. The following remarks sustain this hypothesis:

- It was observed that while the amplitude of the large peaks are non linearly related to the ultrasound transducer drive signal, a threshold level has to be reached in order to observe the signal in plot #8;
- Cavitation bubbles are created during the decompression phase of the ultrasound pressure cycle. The presence of these bubbles would lead to a reduction in the conductivity of the solution, thus producing a large AEI waveform in plot #8. Since there are no equivalent

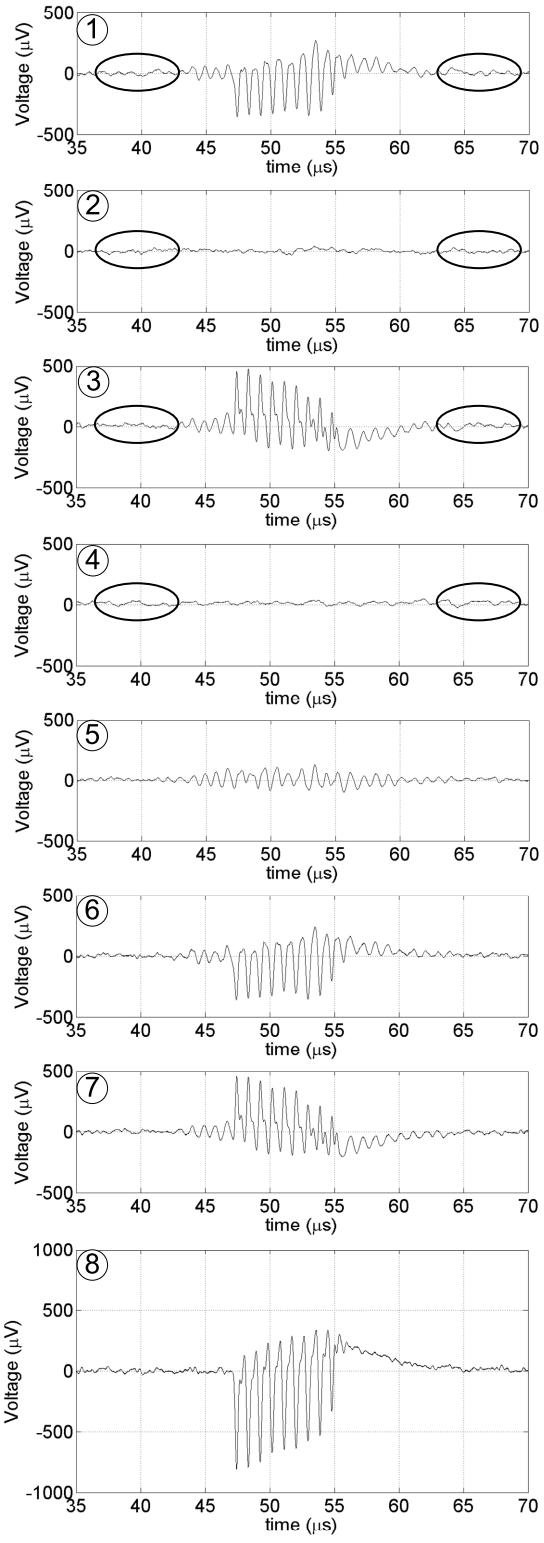

Fig. 3. Acquisition sequence signals. (1)-(5) Acquisitions specified in Table I. (6) Subtraction of the signal (2) from the signal (1) to remove the signal present with the active acquisition system at the positive peak of the current waveform, but without ultrasound. (7) Subtraction of the signal (4) from the signal (3) to remove the signal present with the active acquisition system at the negative peak of the current waveform, but without ultrasound. (8) AEI signal obtained after subtracting the signal taken at the negative peak of the current waveform (signal (7)) from the one taken at the positive peak (signal (6)). All amplitude scales correspond to the magnitude of the signals referred to the input of the amplifiers.

counterparts in the compression phase, there would be no opposite peaks. Note also that the waveform starts abruptly, which is consistent with a threshold effect phenomenon.

The model presented in (5), which forms the basis of our measurements of the electrical conductivity by AEI, does not include the complex cavitation phenomenon we believe we observed. Therefore the presence of gas bubbles would lead to errors if the measurements are interpreted in terms of the intrinsic electrolyte conductivity property we are seeking. Avoiding this could be done using an ultrasonic pressure amplitude below the cavitation threshold (unfortunately also leading to smaller AEI signals) or by using a "unipolar" compressive pulse, as suggested in [6].

As a final remark, comparing plots #8, #6 and #7, we can see that the Debye effect has been effectively removed by the subtraction of the signals taken with different current polarities: small oscillations before and after the burst have nearly disappeared.

B. In vivo considerations

The experimental setup presented in this paper must be partially modified before in vivo imaging can be envisaged. For example, the frequency and amplitude selected for the excitation current, 4.2 $\mathrm{mA_{rms}}$ at 100 Hz, is not suitable for in vivo applications since, under certain conditions, the current could be perceived by some individuals. Biomedical equipment that applies current with body surface electrodes in order to measure a physiological variable (e.g. bio-impedance analyzers, electrocardiographs with circuits that sense detached electrodes, etc.) generally use the safe current limit defined in the standard IEC60601-1 [9]. This specifies a maximum applied current of 100 $\mu\mathrm{A_{rms}}$ for frequencies less or equal to 1 kHz, an increase of 100 $\mu\mathrm{A_{rms}}$ per kHz up to 100 kHz, with a maximum of 10 $\mathrm{mA_{rms}}$ beyond 100 kHz. By redesigning the synchronization circuits so that AEI signals are acquired from single ultrasound cycles reaching the region of interest at the peaks of the sinusoidal current waveforms, it will be possible to increase significantly the excitation frequency. Further refinement of the potential measurement circuits should make it possible to achieve the same signal-to-noise ratio in AEI observations with a much lower excitation current. With both improvements, we believe that the frequency-amplitude combination for the excitation current can be made to comply with the safe current limit defined by the standard IEC60601-1.

For in vivo diagnostic applications, tissue damage that could result from cavitation also needs to be prevented. Safety recommendations on diagnostic medical ultrasonic equipment [10] suggest a maximal mechanical index of 1.9 and therefore limit the maximal rarefaction pressure peak to about 2 MPa for a frequency of 1.078 MHz. The method suggested above to produce a dominant compressive pressure pulse should be constrained to this requirement.

V. CONCLUSIONS AND FUTURE WORK

We have presented an experimental setup and associated instrumentation and methods to acquire and process small AEI signals. Our results show that it is possible to measure the Debye effect and observe small AEI signals with this setup. Our results are consistent with those in the literature and have raised a number of questions related to more subtle effects. Some of these may originate from cavitation, which would have to be avoided for in vivo imaging.

The effect of the size of the measurement domain on the AEI signal amplitude has to be evaluated. We propose to construct AEI sensitivity maps from measurements taken at different positions of the ultrasonic perturbation. Such maps are essential for interpreting the experimental observations and predicting the performance of an acousto-electric imaging system.

The development of a forward model implementing equation (5) for the geometry of the cell and for the acoustic field set by the transducer is needed. We currently have a 2D model, but its extension to 3D now appears essential. Currently, using our 2D forward problem model, we have developed a method to solve the inverse problem that reconstructs the conductivity distributions from simulated AEI signals. We propose to extend this model to 3D and validate it with experimental data acquired with the system described in this paper.

VI. ACKNOWLEDGMENTS

The authors thank Steve Dube for his technical assistance. We acknowledge the support of the Fonds Quebecois de la Recherche sur la Nature et les Technologies, the Natural Sciences and Engineering Research Council of Canada and the Canada Foundation for Innovation.

REFERENCES

[1] B. Lavandier, J. Jossinet and D. Cathignol, "Experimental Measurement of the Acousto-Electric Interaction Signal in Saline Solution", *Ultrasonics*, vol. 38, 2000, pp. 929-936.

[2] H. Zhang and L. V. Wang, "Acousto-Electric Tomography", *Photons Plus Ultrasound : Imaging and Sensing, Proc. of the SPIE*, vol. 5320, 2004, pp. 145-149.

[3] R. Olafsson, R. S. Witte, S.-W. Huang and M. O'Donnell, "Ultrasound Current Source Density Imaging", *IEEE Trans. Bio. Eng.*, vol. 55, 2008, pp. 1840-1848.

[4] R. Witte, R. Olafsson and S.-W. Huang, "Imaging Current Flow in Lobster Nerve Cord using the Acoustoelectric Effect", *Appl. Phys. Lett.*, vol. 90, 2007, p. 163902.

[5] A. J. Surowiec, S. S. Stuchly, J. R. Barr and A. Swarup, "Dielectric Properties of Breast Carcinoma and the Surrounding Tissues", *IEEE Trans. Bio. Eng.*, vol. 35, 1988, pp. 257-263.

[6] B. Lavandier, J. Jossinet and D. Cathignol, "Quantitative Assessment of Ultrasound-Induced Resistance Change in Saline Solution", *Med. Biol. Eng. Comput.*, vol. 38, 2000, pp. 150-155.

[7] J. Jossinet, B. Lavandier and D. Cathignol, "Impedance Modulation by Pulsed Ultrasound", *Annals of the New York Academy of Sciences*, vol. 873, 1999, pp. 396-407.

[8] J. Jossinet, B. Lavandier and D. Cathignol, "The Phenomenology of Acousto-Electric Interaction Signals in Aqueous Solutions of Electrolytes", *Ultrasonics*, vol. 36, 1998, pp. 607-613.

[9] Medical electrical equipment - General requirements for basic safety and essential performance: International Standard IEC60601-1. International Electrotechnical Commission, Geneva, Switzerland, 2005.

[10] Guidelines for the Safe Use of Diagnostic Ultrasound. Minister of Public Works and Government Services Canada, Canada, 2001.